

Semester Project: Magnetic Detumbling Control of a Spacecraft Using Magnetorquers

Ian L. Cooke*

University of Colorado Boulder, Boulder, CO 80309

This project deals with implementing two types of b-dot control laws to a tumbling spacecraft in LEO by applying magnetic torques derived from Earth's magnetic field. The work in this paper approaches the problem by deriving a series of analytic expressions, creating an RK4-based numerical integrator, modeling the Earth's magnetic field, implementing the control laws, performing an orbital inclination performance analysis, and running Monte Carlo simulations. The results were mixed; certain tumbling initial conditions proved to converge quickly, within 2 orbits, while others took much longer. Orbital inclination had minimal effect on convergence, and the Monte Carlo simulations showed that more than half of the initial conditions did not result in convergence. These control laws work well for spacecraft with low angular tumble rates but larger torque rods or better methods of control are needed for larger initial tumbling angular rates.

I. Introduction

THIS paper details the magnetic detumbling of a spinning spacecraft using magnetorquers. The spacecraft has been inserted into a circular Low Earth Orbit (LEO). The motion is assumed to be two-body. A control law will be implemented to reduce the tumbling spacecraft's angular velocity below a desired threshold. This control law will generate a magnetic dipole which will provide the torque that will detumble the spacecraft. This will be achieved via by completing 7 different project milestones. These milestones are

1. Coordinate frame relations
2. Numerical integration
3. Geomagnetic modeling of Earth's magnetic field
4. Nonlinear control law implementation
5. Orbital inclination v/s control performance analysis
6. Monte Carlo Analysis

These project milestones will be achieved using analytic derivations and software implementation.

II. Problem Statement

The spacecraft has been placed into a circular LEO with altitude $h = 450 \text{ km}$ and orbit radius $r = R_{\text{Earth}} + h = 6378 \text{ km} + 450 \text{ km} = 6828 \text{ km}$. The craft is tumbling with initial angular velocity $\omega_{B/N}$. The orbit has inclination i , right ascension of the ascending node Ω , and angle $\theta = \omega + \nu$, but this will just be the true anomaly ν since ω is undefined for circular orbits. The angular rate of the orbit is $\dot{\theta} = \sqrt{\mu/r^3}$, with $\mu = 398\,600 \text{ km}^2/\text{s}^2$. Additionally, the magnetorquers are placed along the principal axes of the spacecraft.

*Student, Spacecraft Attitude Dynamics and Control, CU Boulder Department of Aerospace Engineering Sciences. Student Member of AIAA.

A. Coordinate Frame Definitions

There are 4 different frames necessary for this project:

1. Inertial reference frame $N = \{O, \hat{n}_1, \hat{n}_2, \hat{n}_3\}$
2. Geomagnetic Earth fixed frame $M = \{O, \hat{m}_1, \hat{m}_2, \hat{m}_3\}$
3. LVLH orbit reference frame $H = \{O, \hat{i}_r, \hat{i}_\theta, \hat{i}_h\}$
4. Satellite body fixed reference frame $B = \{H, \hat{b}_1, \hat{b}_2, \hat{b}_3\}$

The LVLH and body reference frames are depicted with the inertial reference frame in Figure 1.

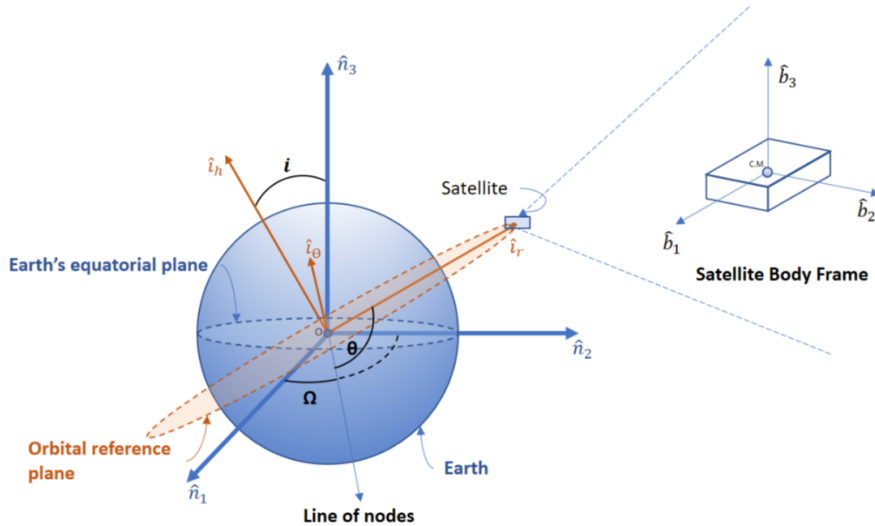


Figure 1: LVLH and Body Reference Frames

The inertial frame has origin at the center of the Earth with the $\hat{n}_1 - \hat{n}_2$ plane as the Earth's equatorial plane and the \hat{n}_3 axis pointing towards the geographic north pole. The LVLH rotating coordinate frame has axis \hat{i}_r tracking the satellite's position along the orbit and \hat{i}_h axis along the orbit angular momentum vector. Then $\hat{i}_\theta = \hat{i}_h \times \hat{i}_r$. The LVLH frame has the (3-1-3) Euler angle set $\{\Omega, i, \theta\}$, where $\theta = \nu$ since the argument of perapse ω is undefined. The satellite body reference frame has origin at the satellites center of mass (CM) and has axes aligned with its principal inertia axes. It is given through the (3-1-3) Euler angle set $\{\psi, \theta, \phi\}$, however the attitude of the body frame relative to the inertial frame will be represented with Modified Rodriguez Parameters (MRPs) given by $\sigma_{B/N} = (\sigma_1, \sigma_2, \sigma_3)^T$.

The geomagnetic earth-fixed (M) frame is depicted in Figure 2.

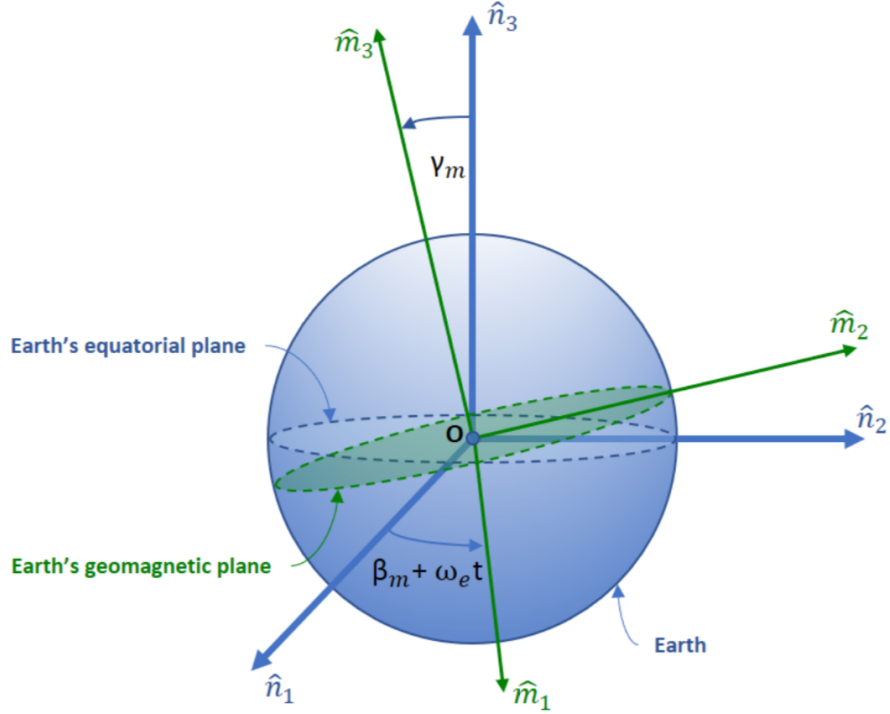


Figure 2: Earth-fixed geomagnetic frame M relative to inertial reference frame N

The M frame has origin at the center of the earth with the axis \hat{m}_3 pointed along Earth's magnetic dipole and $\hat{m}_1 - \hat{m}_2$ plane as the geomagnetic equatorial plane. The \hat{m}_3 axis has constant tilt angle to the \hat{n}_3 axis $\gamma_m = 17$ deg. The angle between the \hat{m}_1 axis and the \hat{n}_1 axis is given by $\beta_m = \beta_{m_0} + \omega_e t$, where $\beta_{m_0} = 0$ deg and $\omega = 7.2921159 \times 10^{-5}$ rad/s is the rotation rate of the Earth. The M frame can be described by the (3-1-3) Euler rotation angles $(\beta_m + \omega_e t, \gamma_m, 0)$, relative to the Inertial frame. The magnetic dipole of the Earth is approximated to have a dipole moment of $M = 7.838 \times 10^6$ Tkm³.

The magnetic field as seen by the LVLH frame is given by

$${}^H b = \frac{M}{r^3} \begin{bmatrix} \cos(\dot{\theta}t - \eta_m) \sin(\xi_m) \\ \cos(\xi_m) \\ -2 \sin(\dot{\theta}t - \eta_m) \sin(\xi_m) \end{bmatrix} \quad (1)$$

where

$$\xi_m = \cos^{-1}(\cos(i) \cos(\gamma_m) + \sin(i) \sin(\gamma_m) \cos(\Omega - \beta_m)) \quad (2)$$

and

$$\eta_m = \sin^{-1}(\sin(\gamma_m) \sin(\Omega - \beta_m) / \sin(\xi_m)) \quad (3)$$

B. Initial Conditions

The mass of the spacecraft is 30 kg and its initial MRP, angular velocity, inertia tensor, and LVLH frame initial angles are

$$\sigma_{B/N} = \begin{bmatrix} 0.3 \\ 0.2 \\ 0.4 \end{bmatrix} \quad (4)$$

$$\omega_{B/N} = \begin{bmatrix} 15 \\ 8 \\ 12 \end{bmatrix} \text{ deg/s} \quad (5)$$

$${}^B[I] = \begin{bmatrix} 3.5 & 0 & 0 \\ 0 & 5.0 & 0 \\ 0 & 0 & 8.0 \end{bmatrix} \text{ kg m}^2 \quad (6)$$

$$\{\Omega, i, \theta_{t_0}\} = \{0, 45, 0\} \text{ deg} \quad (7)$$

The detumble threshold is 3 deg/s for each body axis.

The subsequent sections will satisfy the project milestones, and describe expressions for the attitude of the spacecraft in multiple frames, detail the numerical integrator to propagate the state of the spacecraft, model the geomagnetic field, implementation two versions of a B-dot control law, and analysis of such control laws with a Monte Carlo simulation.

III. Sections with New Work

A. Analytical Derivation of Coordinate Frame Relations

The first milestone is to derive analytic expressions for the direction cosine matrices (DCMs) $[BN]$, $[HN]$, $[MN]$, and $[HM]$. These coordinate frame relations will allow for easy translation between the different coordinate frames defined in this project.

The $[BN]$ DCM is given by using the MRP DCM definition.²

$$[BN] = [I_{3 \times 3}] + \frac{8[\tilde{\sigma}]^2 - 4(1 - \sigma^2)[\tilde{\sigma}]}{(1 + \sigma^2)^2} \quad (8)$$

The $[HN]$ DCM is found by using the (3-1-3) Euler angle set $\{\Omega, i, \theta\}$ in the (3-1-3) DCM.

$$[HN] = \begin{bmatrix} \cos \Omega \cos \theta - \sin \Omega \cos i \sin \theta & \sin \Omega \cos \theta + \cos \Omega \cos i \sin \theta & \sin i \sin \theta \\ -\cos \Omega \sin \theta - \sin \Omega \cos i \cos \theta & \cos \Omega \cos i \cos \theta - \sin \Omega \sin \theta & \cos \theta \sin i \\ \sin \Omega \sin i & -\cos \Omega \sin i & \cos i \end{bmatrix} \quad (9)$$

Using $\Omega = 0$ from the Problem Statement, $[HN]$ simplifies to

$$[HN] = \begin{bmatrix} \cos \theta & \cos i \sin \theta & \sin i \sin \theta \\ -\sin \theta & \cos i \cos \theta & \cos \theta \sin i \\ 0 & -\sin i & \cos i \end{bmatrix} \quad (10)$$

Where $\theta = \nu$, the true anomaly.

The $[MN]$ DCM is found by using the (3-1-3) Euler angle set $\{\beta_m, \gamma_m, 0\}$ in the (3-1-3) DCM.

$$[MN] = \begin{bmatrix} \cos \beta_m & \sin \beta_m & 0 \\ -\cos \gamma_m \sin \beta_m & \cos \beta_m \cos \gamma_m & \sin \gamma_m \\ \sin \beta_m \sin \gamma_m & -\cos \beta_m \sin \gamma_m & \cos \gamma_m \end{bmatrix} \quad (11)$$

Finally, the $[HM]$ DCM is found by using the $[HN]$ and $[MN]$ matrices, equations 10 and 11.

$$[HM] = [HN][MN]^T = \begin{bmatrix} \cos \beta_m \cos \theta + \sin \beta_m \cos i \sin \theta & \dots \\ \sin \beta_m \cos i \cos \theta - \cos \beta_m \sin \theta & \dots \\ -\sin \beta_m \sin i & \dots \\ \sin \gamma_m \sin i \sin \theta - \cos \gamma_m \sin \beta_m \cos \theta + \cos \beta_m \cos \gamma_m \cos i \sin \theta & \dots \\ \sin \gamma_m \cos \theta \sin i + \cos \gamma_m \sin \beta_m \sin \theta + \cos \beta_m \cos \gamma_m \cos i \cos \theta & \dots \\ \sin \gamma_m \cos i - \cos \beta_m \cos \gamma_m \sin i & \dots \\ \cos \gamma_m \sin i \sin \theta + \sin \beta_m \sin \gamma_m \cos \theta - \cos \beta_m \sin \gamma_m \cos i \sin \theta & \dots \\ \cos \gamma_m \cos \theta \sin i - \sin \beta_m \sin \gamma_m \sin \theta - \cos \beta_m \sin \gamma_m \cos i \cos \theta & \dots \\ \cos \gamma_m \cos i + \cos \beta_m \sin \gamma_m \sin i & \dots \end{bmatrix}_{(12)}$$

This completes milestone 1.

B. Numerical Integrator

The next milestone is to develop a classic Runge-Kutta (RK4) based numerical integrator to propagate the state

$$\mathbf{X} = \begin{bmatrix} \boldsymbol{\sigma}_{B/N} \\ \boldsymbol{\omega}_{B/N} \end{bmatrix} \quad (13)$$

The dynamics of this numerical integrator will obey the rigid body dynamics equations of motion in Equation 14.

$$[I]\dot{\boldsymbol{\omega}}_{B/N} = -[\tilde{\boldsymbol{\omega}}_{B/N}][I]\boldsymbol{\omega}_{B/N} + \mathbf{u} \quad (14)$$

In order to demonstrate the integrator works, \mathbf{X} was propagated forward 100 seconds with no control torque ($\mathbf{u} = 0$) using the initial conditions given in Section II.B. If the integrator works, then the angular momentum magnitude H and kinetic energy T should be constant. Figure 3 shows H and T for the 100 second propagation. The propagated MRPs and angular velocity components, Figures 27 and ??, respectively, can be found in Appendix A..

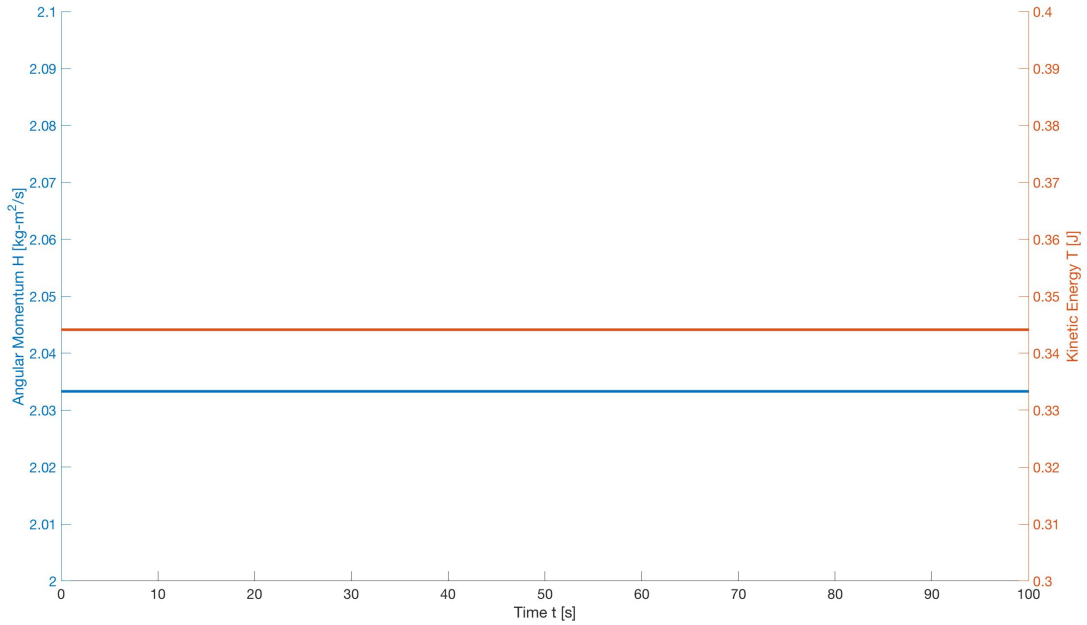


Figure 3: Angular momentum magnitude and kinetic energy without control torque

It is clear from the figure that H and T remain constant for the propagation, and therefore the integrator works. This integrator will be used for the duration of the project to propagate the state \mathbf{X} . This completes the second milestone.

C. Geomagnetic Modeling

It is important to model the Earth's magnetic field since this is the medium by which the satellite will detumble itself. The geomagnetic field as seen by the LVLH frame ${}^H\mathbf{b}$ is shown in Equation 1. Figure 4 shows the local geomagnetic field as seen by the LVLH frame over one orbit, with $\beta_{m_0} = 0$ deg. The orbital period is $T = 2\pi\sqrt{r^3/\mu} = 93.58$ min.

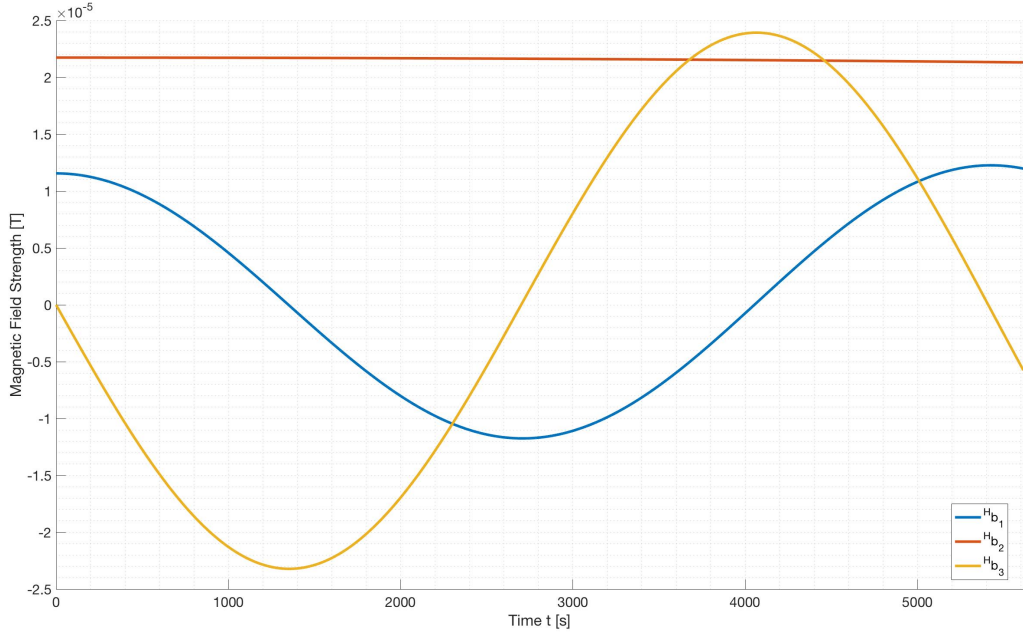


Figure 4: Local magnetic field propagated over one orbit as seen by the LVLH frame

Next, the geomagnetic field in body-frame components, ${}^B\mathbf{b}$, is calculated for 100 seconds. The geomagnetic field in body-frame components is

$${}^B\mathbf{b} = [BH]^H \mathbf{b} \quad (15)$$

where

$$[BH] = [BN][HN]^T \quad (16)$$

The $[BN]$ DCM, given by Equation 8, is calculated using the propagated MRPs, and the $[HN]$ is given by Equation 9. Each DCM is re-calculated for each discrete instance in time. ${}^B\mathbf{b}$ is shown in Figure 5.

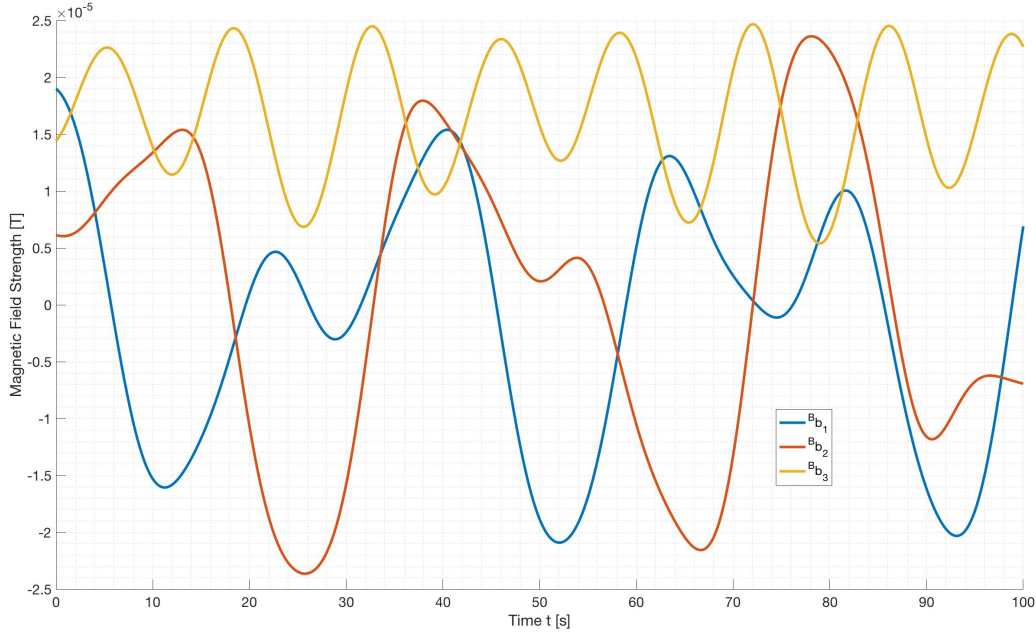


Figure 5: Geomagnetic field in body-frame components calculted for 100 seconds

This completes Milestone 3 of the project. Now that milestones 1 through 3 have been completed, the control laws can be implemented.

D. Milestone 4: Control Law Implementation

There are two distinct b-dot control laws that will be implemented in this project. Both of these control laws are used to calculate the control dipole \mathbf{m} which is used with the magnetic field strength to calculate the actual control torque \mathbf{u} . The first to be implemented is the modulating b-dot control law, and is given by Equation 17.

$$\mathbf{m} = \frac{-k_\omega}{\|\mathbf{b}\|} \hat{\mathbf{b}} \times [(I_{3 \times 3} - \hat{\mathbf{b}}\hat{\mathbf{b}}^T)\boldsymbol{\omega}] \quad (17)$$

Where

$$k_\omega = 2\dot{\theta}(1 + \sin(\xi_m))I_{min} \quad (18)$$

and $\hat{\mathbf{b}}$ is the unit vector pointing in the direction of the local magnetic field in B coordinates.

The control torque is given by Equation 19.

$$\mathbf{u} = \mathbf{m} \times \mathbf{b} \quad (19)$$

The second control law is the bang-bang b-dot control law given by Equation 20.

$$\mathbf{m} = -m_{max} \text{sgn}(\mathbf{b}') \quad (20)$$

Where $m_{max} = 3A - m^2$ is the maximum command dipole the torque rods can provide and \mathbf{b}' is the derivative of the local magnetic field as seen by the body frame. A derivation for \mathbf{b}' can be found in Appendix B.. The control torque is given by Equation 19

Besides the initial conditions given in II.B., two more will be used to analyze the performance of these two control laws, given below.

1.

$$\sigma_{B/N} = \begin{bmatrix} 0.1 \\ 0.1 \\ 0.4 \end{bmatrix} \quad \omega_{B/N} = \begin{bmatrix} 1 \\ 12 \\ 1 \end{bmatrix}_B \text{ deg/s} \quad (21)$$

2.

$$\sigma_{B/N} = \begin{bmatrix} 0.35 \\ 0.2 \\ 0.15 \end{bmatrix} \quad \omega_{B/N} = \begin{bmatrix} 6 \\ 4 \\ 13 \end{bmatrix}_B \text{ deg/s} \quad (22)$$

The objective is to drive the components of the angular rates below 3 deg/s within 3 orbits.

1. Case 1: Mission Overview Conditions and Modulating Control

Figure 6 shows the integrated state which includes the MRPs and angular rates over three orbits, and Figure 7 shows the control torque and command dipole over the same time-span.

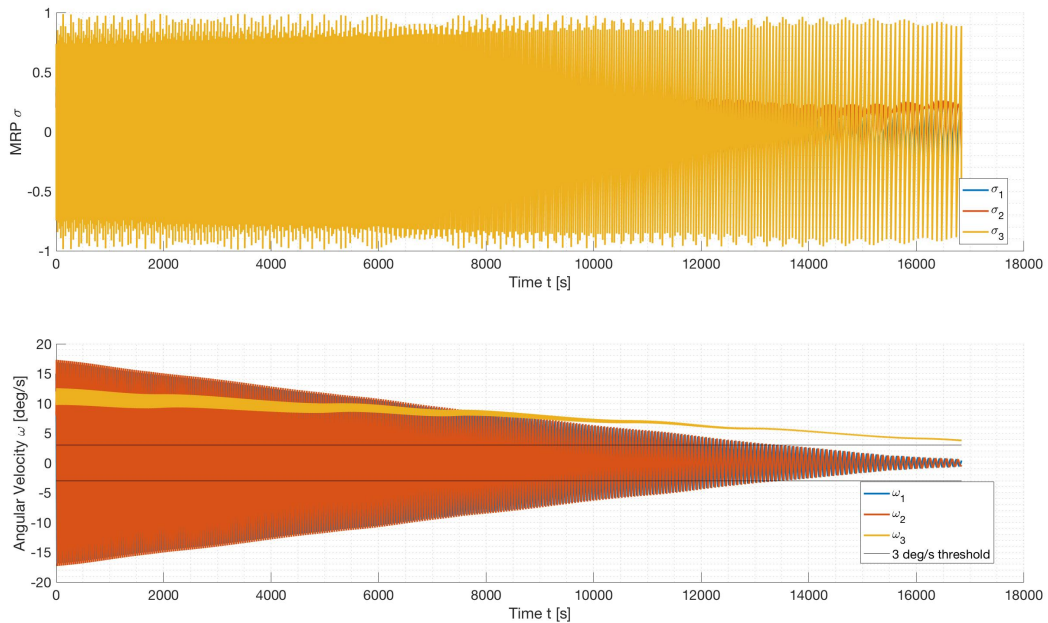


Figure 6: Case 1: Mission Overview Initial Conditions, Modulating Control: Integrated State

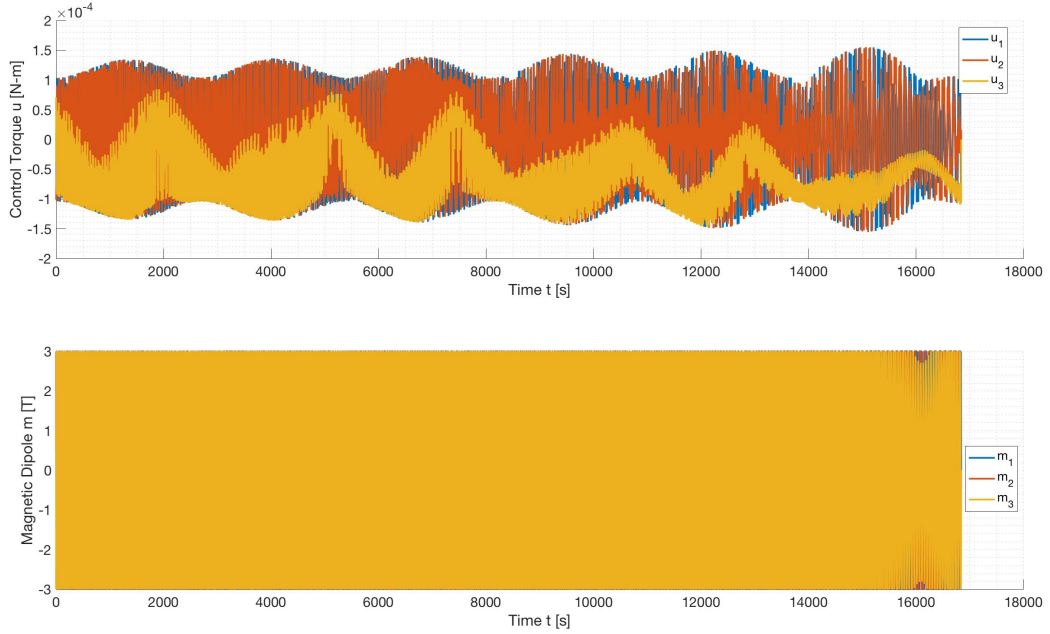


Figure 7: Case 1: Mission Overview Initial Conditions, Modulating Control: Control Torque and Command Dipole

Figure 6 shows that while ω_1 and ω_2 converge within 3 orbits, ω_3 remains just outside the threshold. Figure 7 shows that the command dipole is completely maxed out for almost the entire duration of the simulation. This is because the control torque is very weak; on the order of $1e^{-5}$ N – m.

2. Case 2: Mission Overview Conditions and Bang-Bang Control

Figure 8 shows the integrated state which includes the MRPs and angular rates over three orbits, and Figure 9 shows the control torque and command dipole over the same time-span.

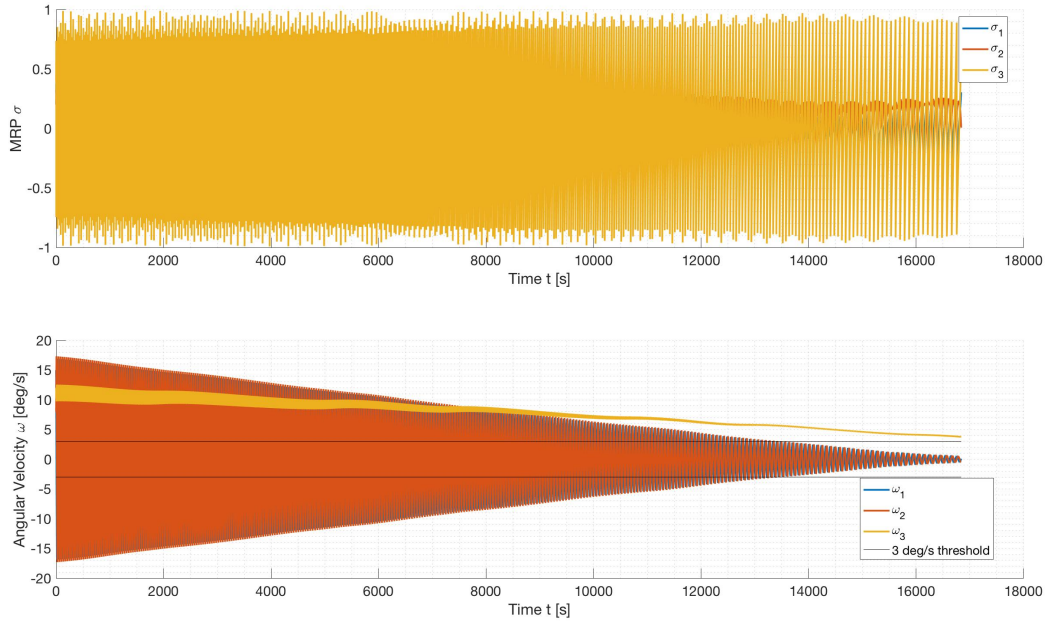


Figure 8: Case 2: Mission Overview Initial Conditions, Bang-Bang Control: Integrated State

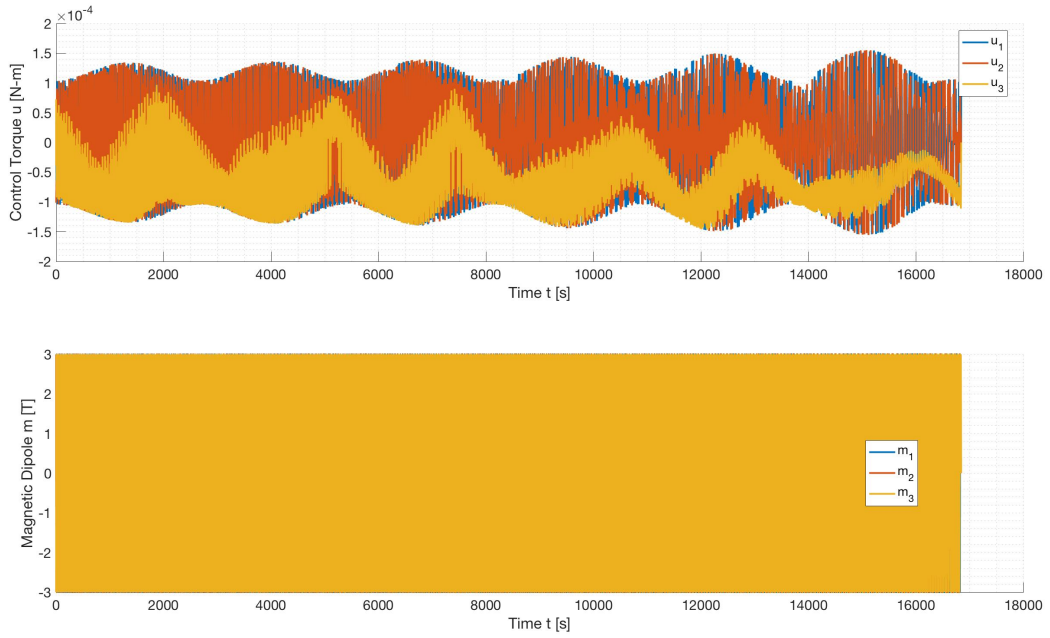


Figure 9: Case 2: Mission Overview Initial Conditions, Bang-Bang Control: Control Torque and Command Dipole

Remarkably, the bang-bang control upon inspection is almost identical to that of the modulating law. For further investigation, a plot of the difference in the angular velocity components produced by Case 1

and Case 2 is provided in Figure 10.

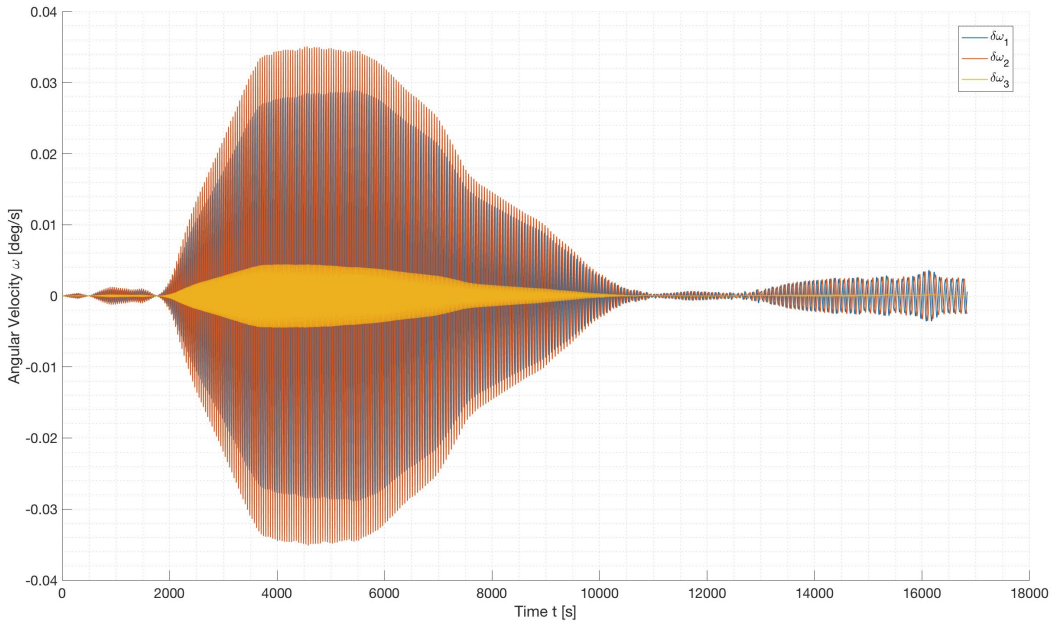


Figure 10: Difference in Angular Velocity Components for Case 1 and Case 2

Just as in Case 1, Figure 8 shows that while ω_1 and ω_2 converge within 3 orbits, ω_3 remains just outside the threshold. The command dipole is also virtually maxed out in this case.

3. Case 3: Initial Condition 1 and Modulating Control

Figure 11 shows the integrated state which includes the MRPs and angular rates over three orbits, and Figure ?? shows the control torque and command dipole over the same time-span.

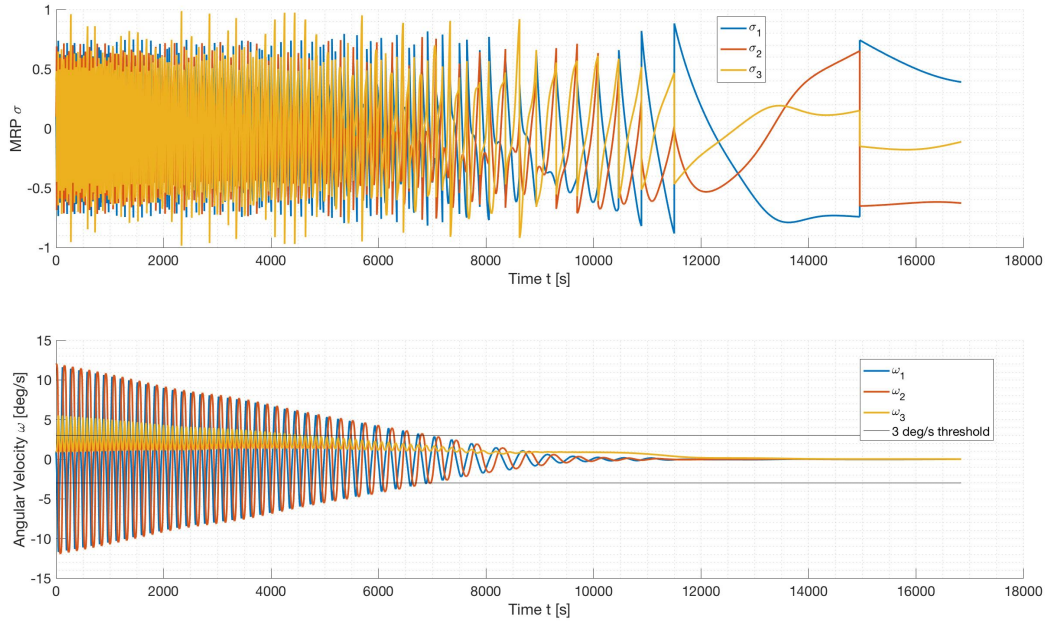


Figure 11: Case 3: Initial Condition 1, Modulating Control: Integrated State

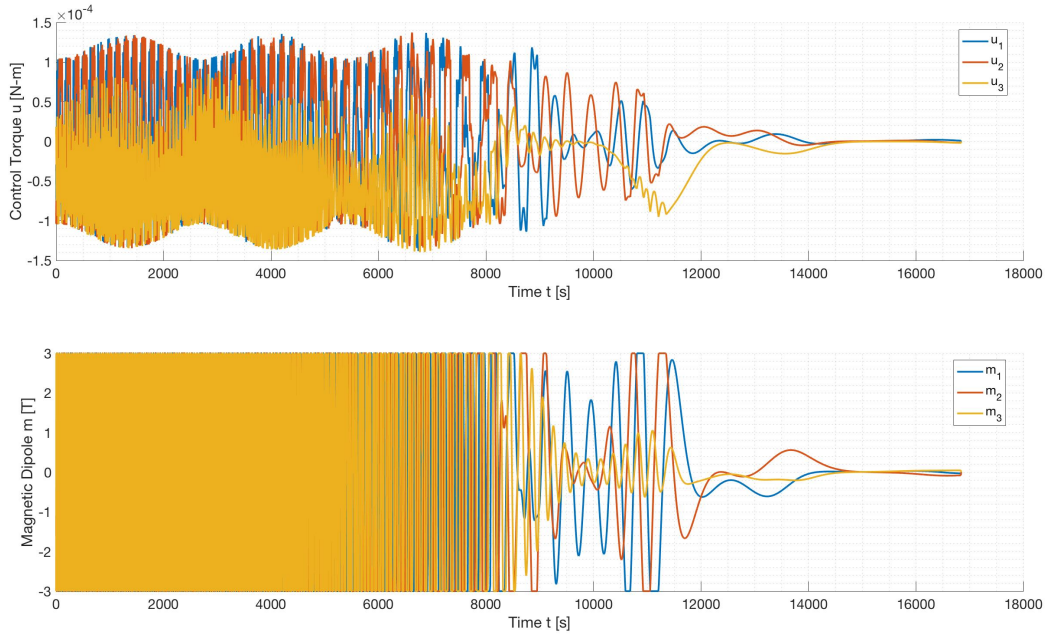


Figure 12: Case 3: Initial Condition 1, Modulating Control: Control Torque and Command Dipole

All components of angular velocity converge to the threshold within about 117 minutes, or 1.25 orbits, and once converged the control torque and command dipole also clearly diminish.

4. Variation of Gains for Case 3

For this Case the gain k_ω was also varied to understand how it affected performance. Instead of using the definition in Equation 18, the gains were set at 0.0005 and 0.001. The maximum gain attained during Case 3 with Equation 18 was found to be 0.0132. Increasing the gain had virtually zero impact on the results since the command dipole is essentially maxed out, and only by reducing the gain by an order of magnitude was there a noticeable change in the result. Figure 13 shows the angular velocities from implementation of $k_\omega = 0.0005$ while Figure 14 shows the implementation of the $k_\omega = 0.001$.

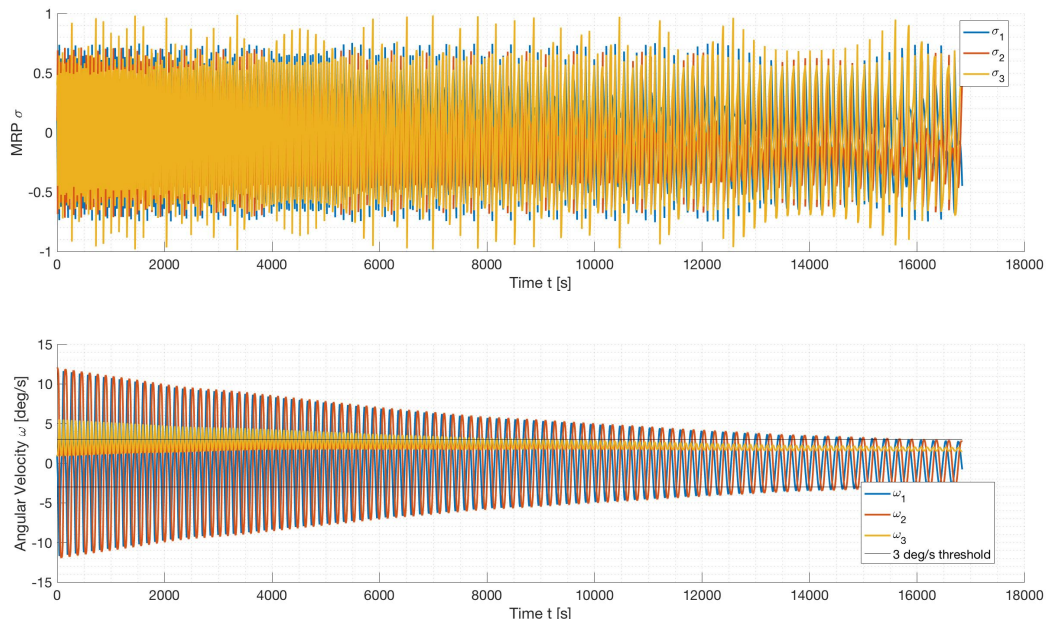


Figure 13: Case 3: Implementation of gain 0.0005

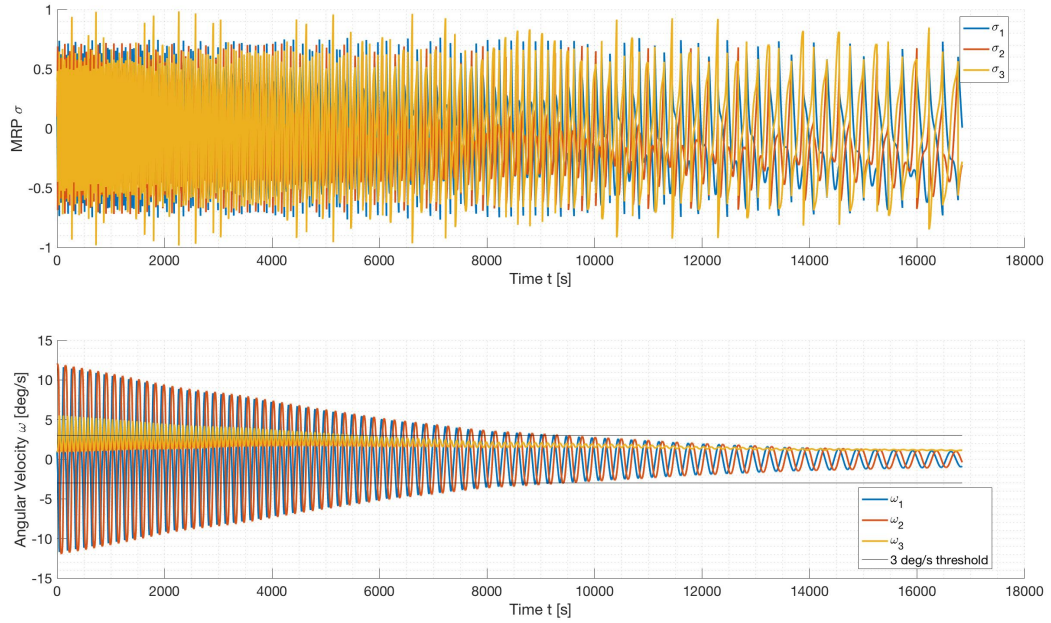


Figure 14: Case 3: Implementation of gain 0.001

Now, the gain of 0.0005 just barely causes the angular rates to converge in 3 orbits while the gain of 0.001 causes the rates to converge in just over 2 orbits.

5. Case 4: Initial Condition 1 and Bang-Bang Control

Figure 15 shows the integrated state which includes the MRPs and angular rates over three orbits, and Figure 16 shows the control torque and command dipole over the same time-span.

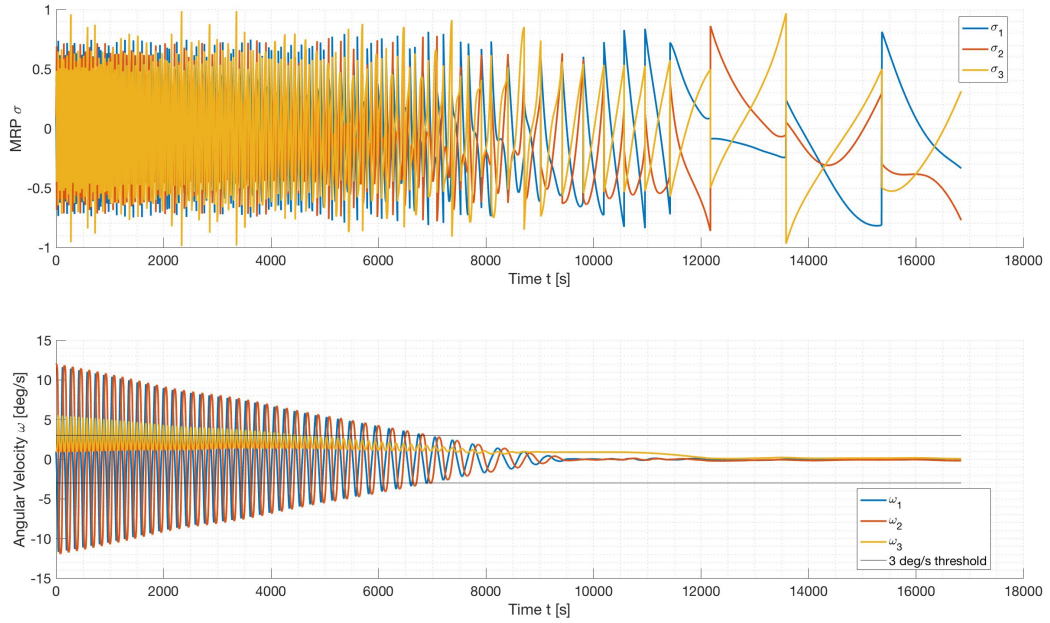


Figure 15: Case 4: Initial Condition 1, Bang-Bang Control: Integrated State

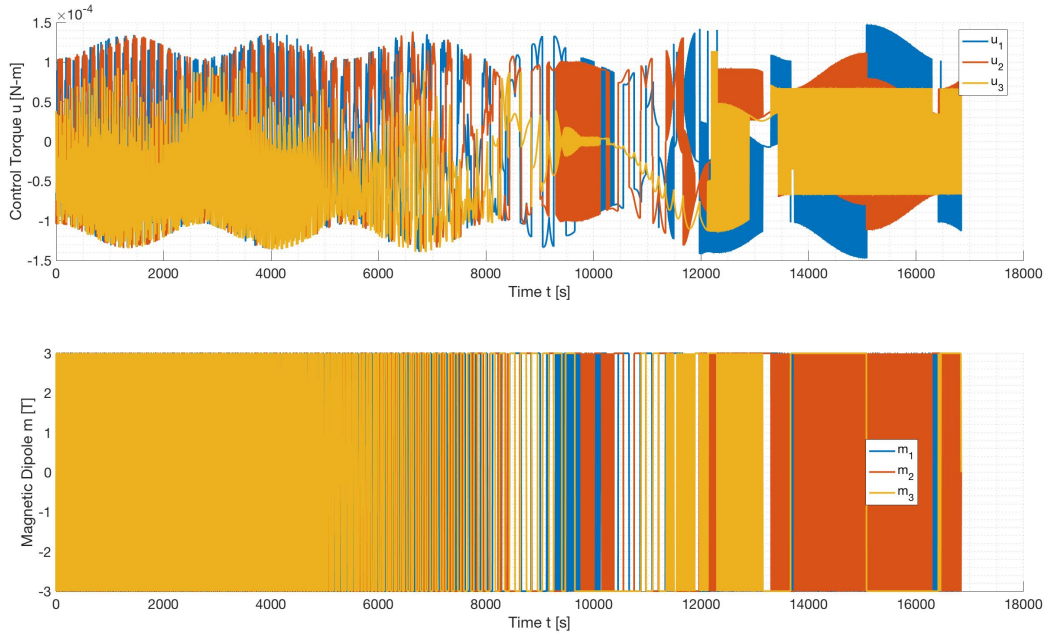


Figure 16: Case 4: Initial Condition 1, Bang-Bang Control: Control Torque and Command Dipole

Just as in cases 1 and 2, the bang-bang control is remarkably similar to the modulating control and converges in almost exactly the same amount of time.

6. Case 5: Initial Condition 2 and Modulating Control

Figure 17 shows the integrated state which includes the MRPs and angular rates over three orbits, and Figure 18 shows the control torque and command dipole over the same time-span.

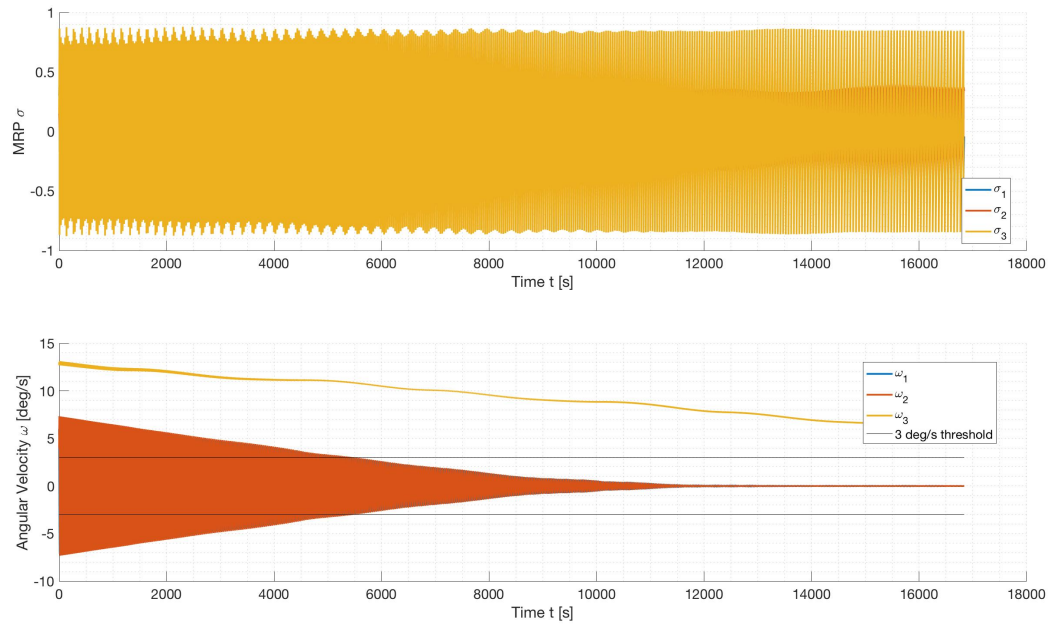


Figure 17: Case 5: Initial Condition 2, Modulating Control: Integrated State

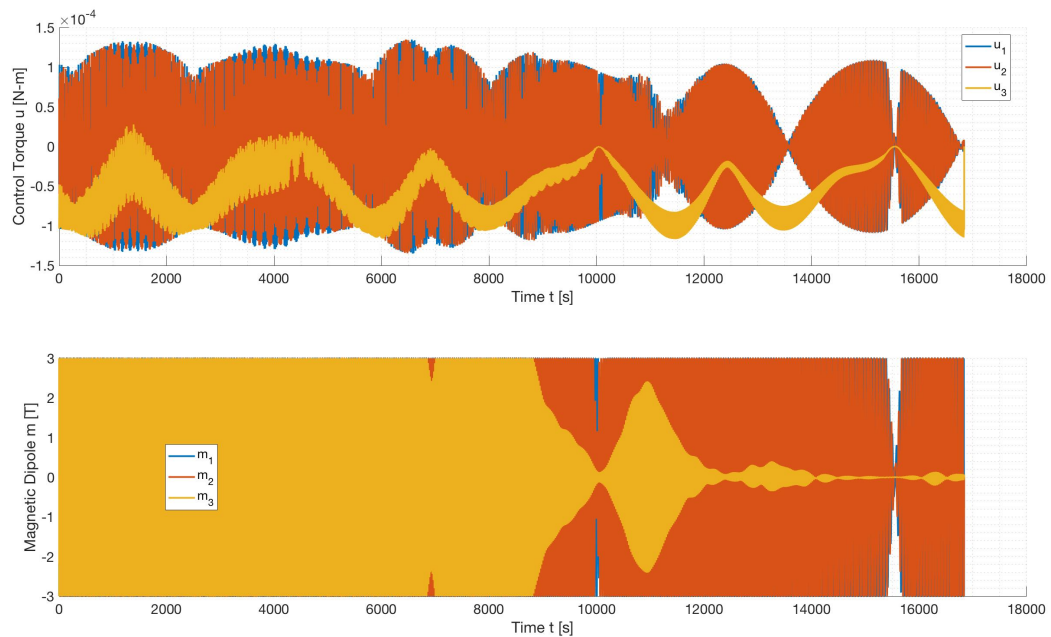


Figure 18: Case 5: Initial Condition 2, Modulating Control: Control Torque and Command Dipole

Just as in case 1 and 2, the angular rate components ω_1 and ω_2 converge relatively quickly, almost within an orbit, but the ω_3 component does not converge below the threshold within the 3-orbit restraint.

7. Case 6: Initial Condition 2 and Bang-Bang Control

Figure 19 shows the integrated state which includes the MRPs and angular rates over three orbits, and Figure 20 shows the control torque and command dipole over the same time-span.

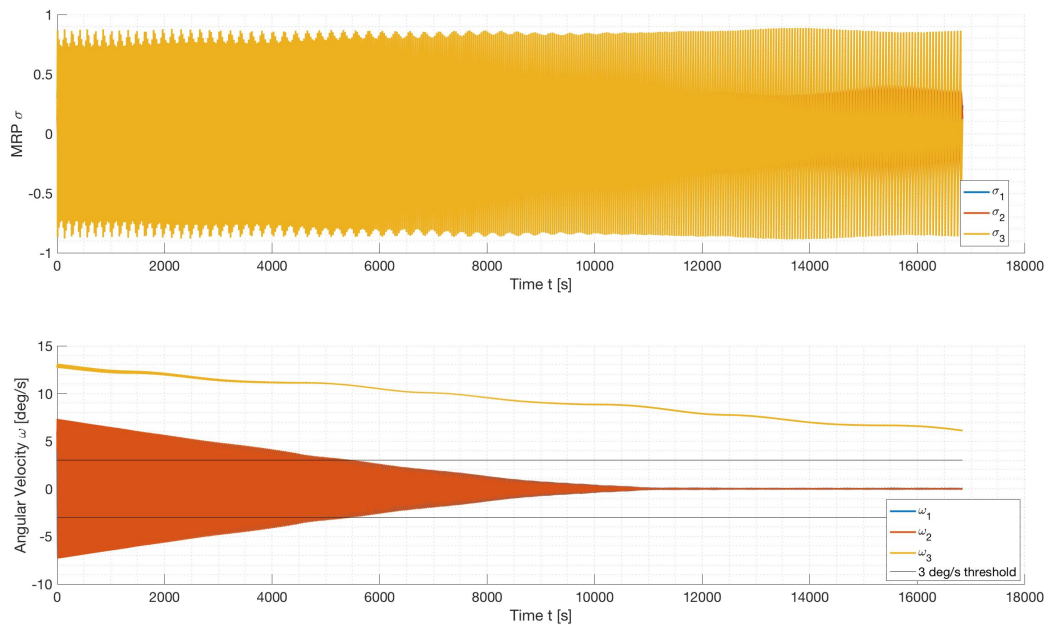


Figure 19: Case 6: Initial Condition 2, Bang-Bang Control: Integrated State

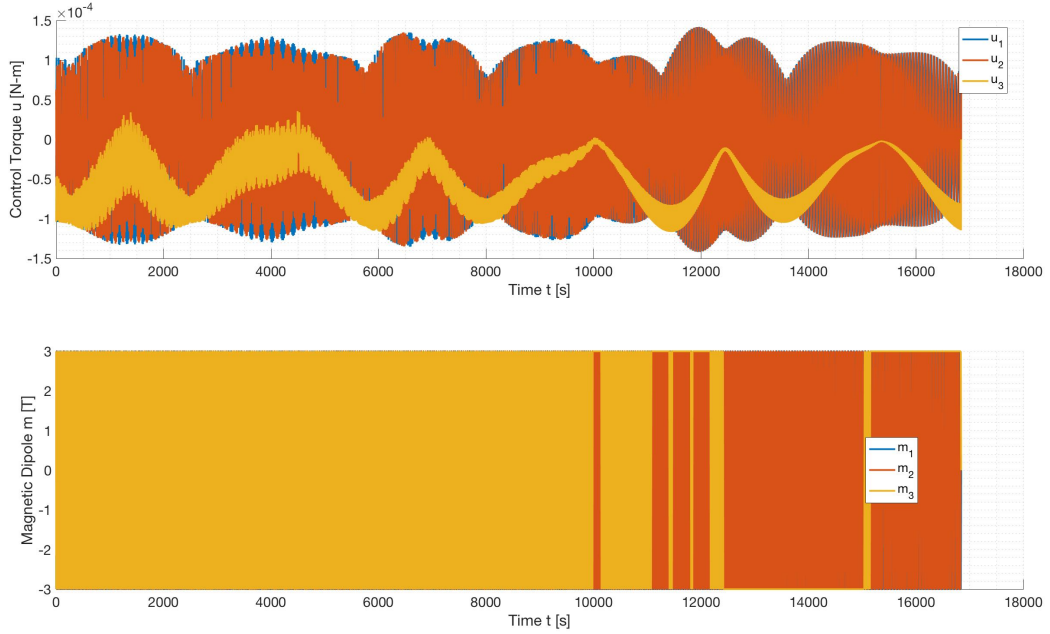


Figure 20: Case 6: Initial Condition 2, Bang-Bang Control: Control Torque and Command Dipole

Just as in cases 1 and 2, and 3 and 4, the bang-bang control is remarkably similar to the modulating control and converges in almost exactly the same amount of time.

E. Milestone 5: Orbit Inclinations v/s Control Performance

Since the magnetic field is dependent on the spacecraft's orbital inclination and the control law is dependent on the magnetic field, this section explores the performance of the control laws versus the orbital inclination. Two orbital inclinations will be studied, 15 deg and 105 deg. The gain will be reset to that given in Equation 18. The initial conditions will be from Section II.B..

1. Case 1: 15 deg Orbital Inclination and Modulating Control

Figure 21 shows the propagated state for the 15 deg inclination and modulating control case.

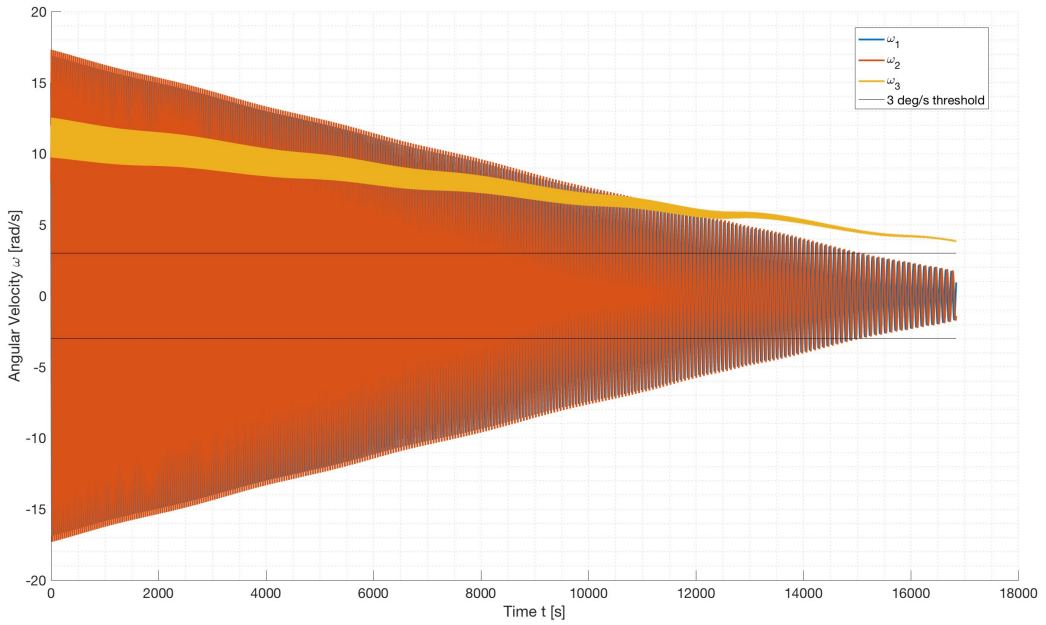


Figure 21: Case 1: 15 deg Orbital Inclination and Modulating Control: Propagated State

Almost identical to Case 1 of Milestone 4, only 2 out of the 3 angular rate components converge.

2. Case 2: 15 deg Orbital Inclination and Bang-Bang Control

Figure 22 shows the propagated state for the 15 deg inclination and bang-bang control case.

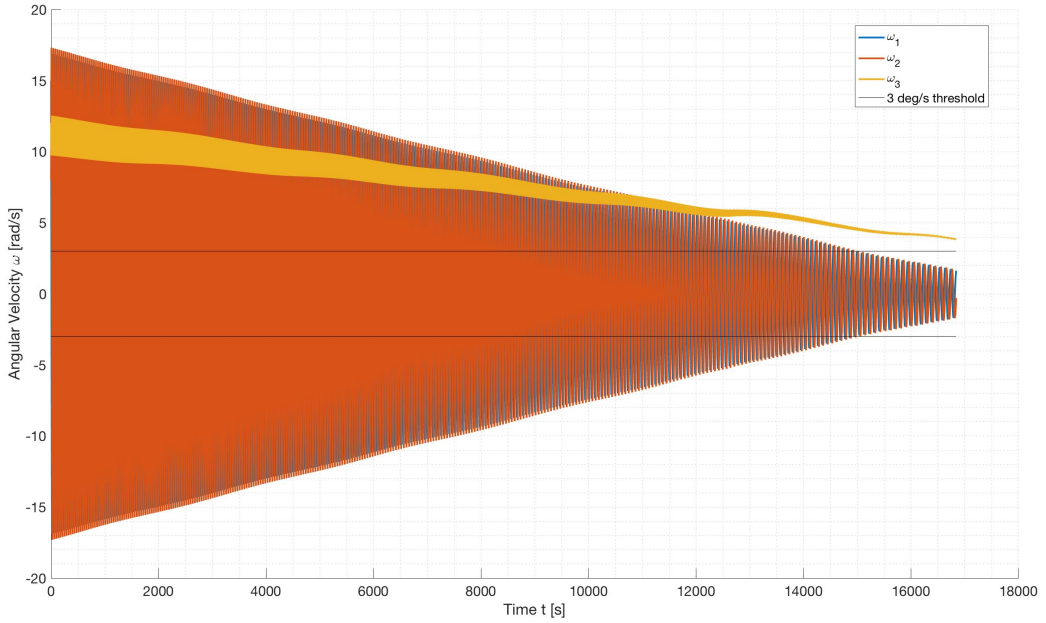


Figure 22: Case 2: 15 deg Orbital Inclination and Bang-Bang Control: Propagated State

Almost identical to Case 1 of this milestone, only 2 out of 3 angular rates converge. It is clear that adjusting the inclination to 15 degrees has little effect on the convergence of the angular rates.

3. Case 3: 105 deg Orbital Inclination and Modulating Control

Figure 23 shows the propagated state for the 105 deg inclination and modulating control case.

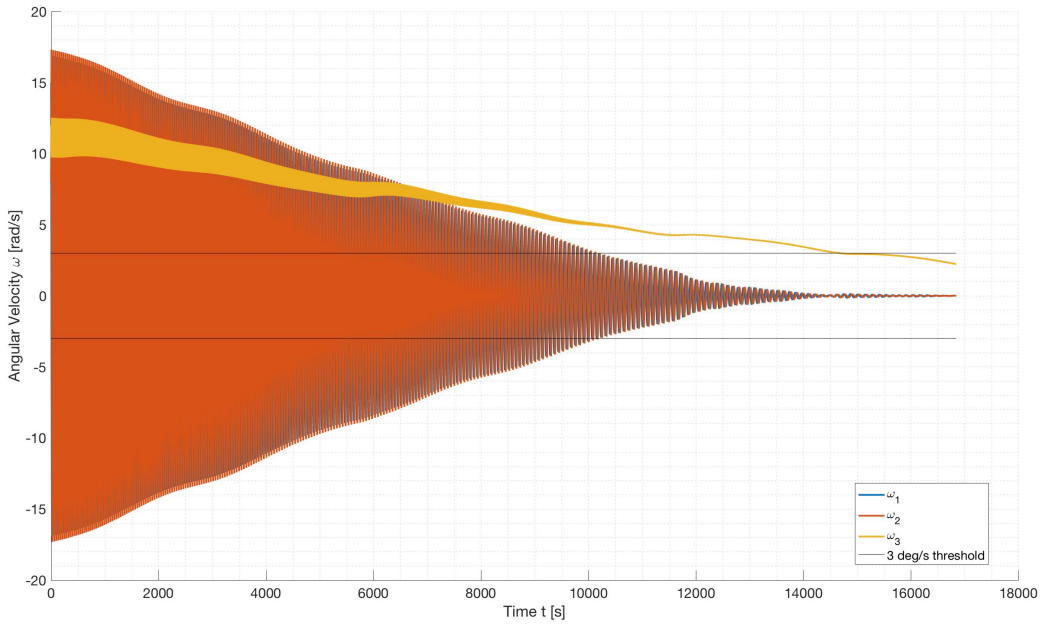


Figure 23: Case 3: 105 deg Orbital Inclination and Modulating Control: Propagated State

Changing the orbital inclination to 105 deg does cause the third angular rate to converge along with the other 2, but just barely within the 3-orbit constraint.

4. Case 4: 105 deg Orbital Inclination and Bang-Bang Control

Figure 24 shows the propagated state for the 105 deg inclination and bang-bang control case.

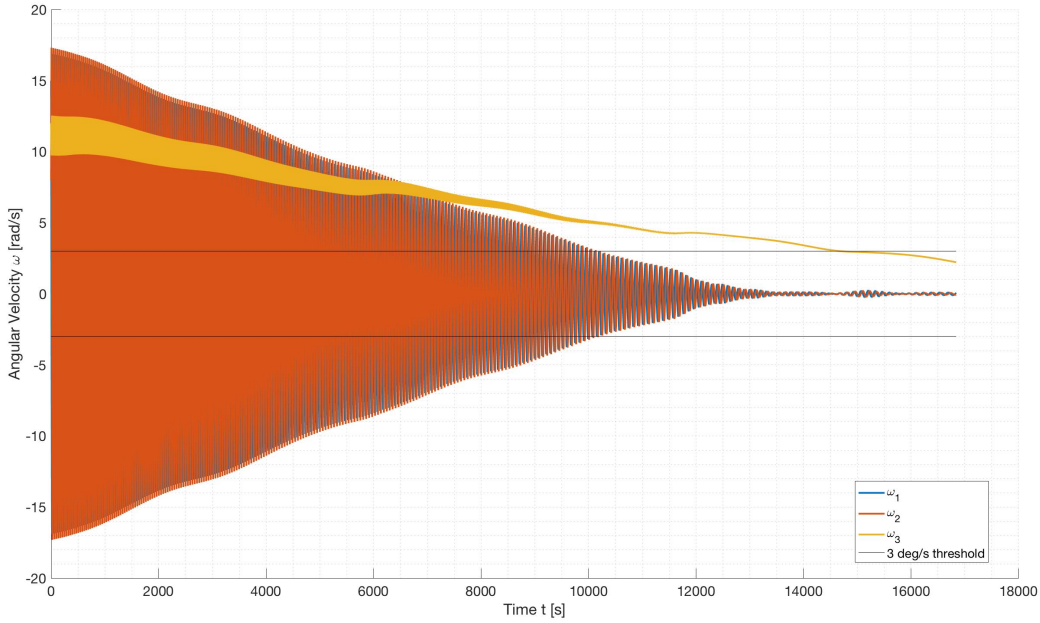


Figure 24: Case 4: 105 deg Orbital Inclination and Bang-Bang Control: Propagated State

As expected, this result is nearly identical to Case 3 of this milestone.

One further exploration in this analysis was to determine the minimum dipole necessary for each control law in the 15 deg case to cause the angular rates to converge to within 1 deg/s within 3 orbits. For the modulating law, this was found to be 4.33, and for the bang-bang case, this was found to be 4.16.

F. Milestone 6: Monte Carlo Analysis

The final milestone of this project is to complete a Monte Carlo simulation for each control law from a randomly generated initial condition and observe the results. The maximum magnetic dipole for each axis was also increased to $4 \text{ A} - \text{m}^2$. For each law, 25 simulations were conducted. Each simulation used a random angular rate initial condition given by

$$10 \text{ deg/s} < |\omega_{B/N(i)}| < 16 \text{ deg/s} \quad (23)$$

The results of this simulation for the modulating control law are contained in Figure 25 and the results for the bang-bang control law are in Figure 26.

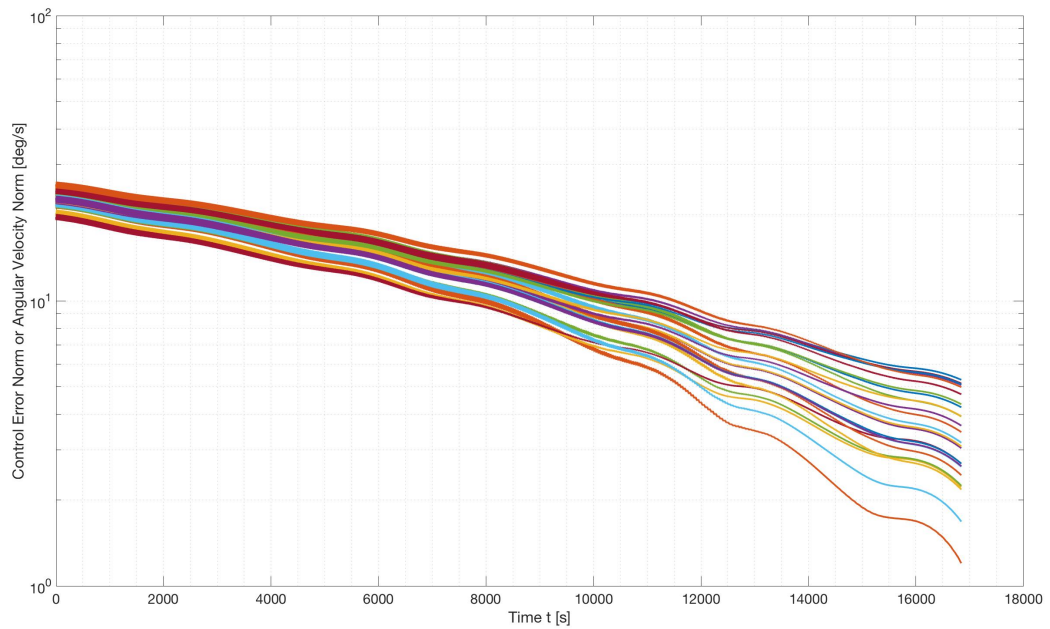


Figure 25: Monte Carlo Simulation for Modulating Control

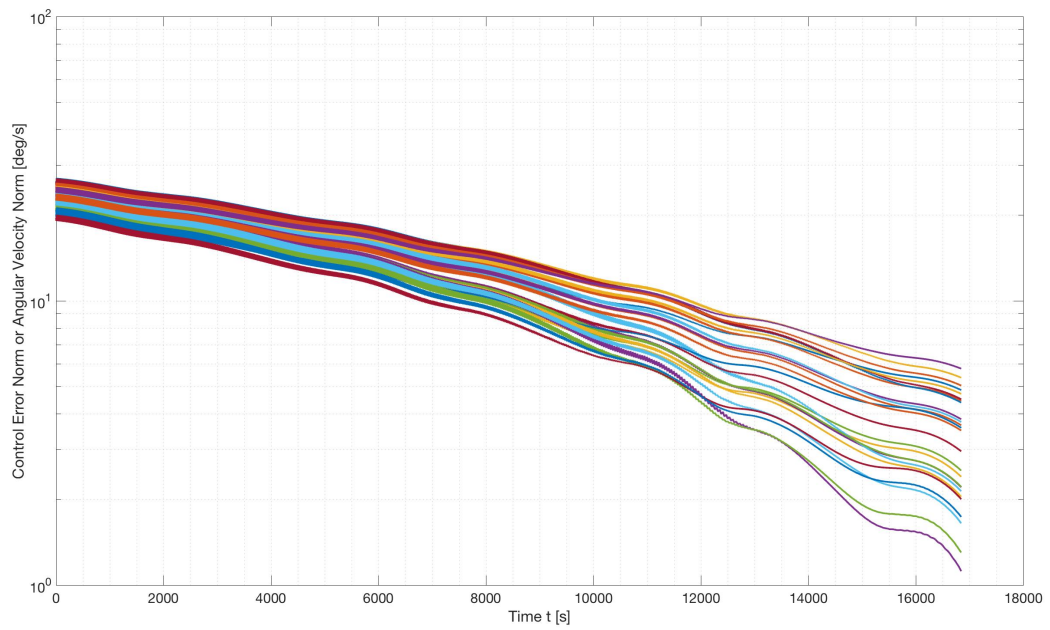


Figure 26: Monte Carlo Simulation for Bang-Bang Control

Overall, the bang-bang control performs very similarly to the modulating control, but even still, less than half of the simulations were able to converge to the threshold of 3 deg/s, even with the increased maximum dipole moment. The expected steady-state error within the time constraint is unquantifiable

because the simulation is not given adequate time to reach steady-state. The same is the case for the settling time.

IV. Conclusion

The conclusion you briefly summarize the paper. Discuss what problem was solved, how it was solved, any limitations of the method. Contrary to the introduction, you do briefly discuss the results here. It is also ok to briefly address future research in this area.

This project dealt with the detumbling of a spacecraft in LEO using Earth's magnetic field, the satellite's magnetorquers, and 2 variations of a b-dot control law. Solving the problem involved simulating Earth's magnetic field in multiple coordinate frames, creating an RK4-based numerical integrator from scratch, and successfully implementing the control laws. An orbital inclination trade study and Monte Carlo simulation were conducted to analyze the performance of the control laws. The control laws turned out to produce remarkably similar results; almost exact. Unfortunately these control laws were not always reliable in detumbling the spacecraft to within the desired threshold, especially evidenced by the Monte Carlo simulations. Further research would need to be conducted on implementing larger torque rods for applying larger magnetic torques or alternative methods of control for detumbling for more reliable results.

References

¹Schaub, Hanspeter. ASEN 5010 Semester Project."

²Appendix B.1 Direction Cosine Matrix in Terms of the 12 Euler Angle Sets. *Analytical Mechanics of Space Systems*, by Hanspeter Schaub and John L. Junkins, 3rd ed., American Institute of Aeronautics and Astronautics, 2009, p. 798.

Appendix

A. RK4 Numerical Integrator

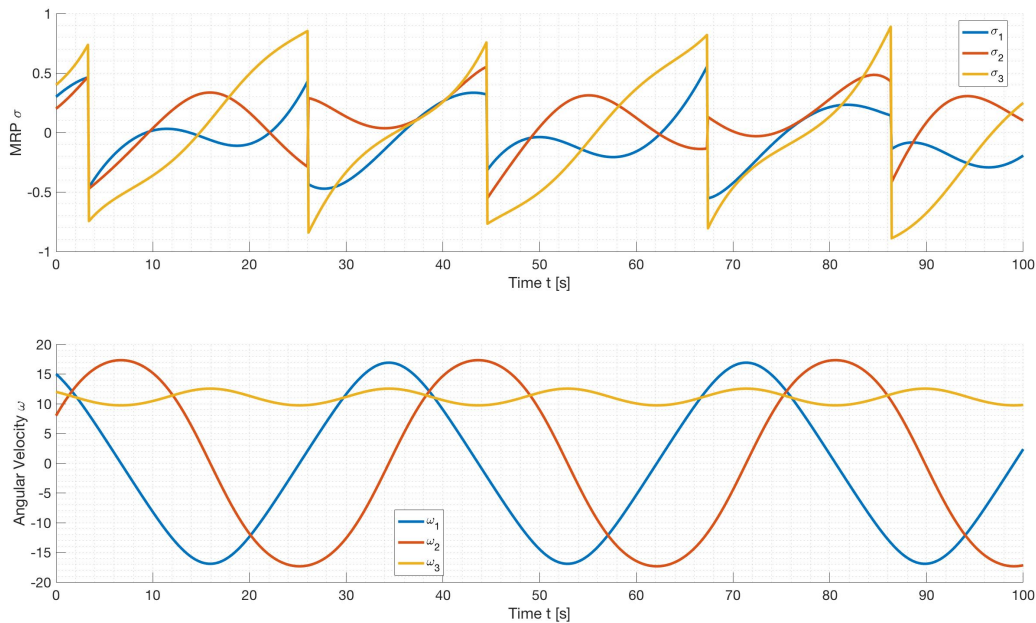


Figure 27: MRPs propagated 100 seconds without control torque

B. Derivation of Magnetic Field Derivative

The quantity of $\dot{\mathbf{b}}$ represents the time derivative of the local magnetic field as seen by the body frame in body frame components. Starting out with an expression for ${}^B\mathbf{b}$,

$${}^B\mathbf{b} = [BH]^H \mathbf{b} \quad (24)$$

and taking the derivative, we have

$$\frac{d}{dt}({}^B\mathbf{b}) = [\dot{BH}]^H \mathbf{b} + [BH]^H \frac{d}{dt}({}^H\mathbf{b}) \quad (25)$$

Using the fact that $[\dot{BH}] = -[\tilde{\omega}_{B/H}][BH]$, we now have

$$\frac{d}{dt}({}^B\mathbf{b}) = (-[\tilde{\omega}_{B/H}][BH])^H \mathbf{b} + BH \frac{d}{dt}({}^H\mathbf{b}) \quad (26)$$

where $-[\tilde{\omega}_{B/H}]$ is written in body-frame components and

$${}^B\boldsymbol{\omega}_{B/H} = {}^B\boldsymbol{\omega}_{B/N} - [BH]^H \boldsymbol{\omega}_{H/N} \quad (27)$$

The angular velocity ${}^H\boldsymbol{\omega}_{H/N} = (0, 0, \dot{\theta})^T$, using the Euler Angle set for the LVLH frame $\{\Omega, i, \theta\}$ and its respective kinematic differential equations, and the fact that the time-derivatives of both Ω and i are equal to 0.

The quantity $\frac{d}{dt}({}^H\mathbf{b})$ is approximated numerically in the simulations due to its complex analytic expression and is given by

$$\frac{d}{dt}({}^H\mathbf{b}) \approx \frac{{}^H\mathbf{b}_{n+1} - {}^H\mathbf{b}_n}{t_{n+1} - t_n} \quad (28)$$